A Fast and Accurate Method for Measuring the Dielectric Constant of Printed Wiring Board Materials

Nicholas G. Paulter

Abstract— **A new time-domain-reflectometry measurement method is described that provides accurate measurements of the average high-frequency (0.1 GHz to 5 GHz) dielectric constant of printed wiring board (PWB) materials and that is suitable for "factory-floor" usage. A parallel-plate transmission line is used for the sample geometry. A model is developed that describes the electrical behavior of the transmission line thereby allowing the dielectric constant to be extracted from the observed signal. The data analysis and the sample preparation are both simple to accomplish.**

Index Terms—**Dielectric materials, factory-floor measurement, permittivity, printed wiring board, time-domain reflectometry.**

I. Introduction

A NEW time-domain measurement method was developed to measure the high-frequency (0.1 GHz to 5 GHz) relative dielectric constant, ϵ_r, values of printed wiring board (PWB) dielectrics using simple sample geometries. PWB's are used as the substrate on which the integrated circuits (IC's) and discrete devices of an electronic product are mounted and electrically interconnected. In certain applications, the PWB interconnect behaves as a transmission line (TL) and, as such, the electrical-wave propagation properties of the TL becomes important. The electrical properties of the PWB TL's are dependent on a variety of variables that include dielectric and conductor properties and the physical dimensions of the TL's. This paper focuses on one of these parameters, ϵ_r. In particular, a frequency-averaged (0.1 GHz to 5 GHz) ϵ_r is found because a scalar is typically used for PWB circuit design and ϵ_r is fairly constant for most PWB dielectrics over this frequency range.

The purpose of the work described in this paper was to develop a measurement technique for determining ϵ_r. Although there are a variety of frequency-domain [1]–[9] and time-domain [10]–[17] methods that have been developed for obtaining ϵ_r, this work is focused on measurement requirements unique to the PWB industry. These measurement requirements are that the technique should be an inexpensive, easy-to-use, robust "factory-floor" measurement system capable of providing immediate results. In addition, sample preparation should be as simple as possible to avoid increased cost of PWB production. Another concern is that ϵ_r as measured by the laminate (metal-clad or unclad dielectric) supplier is often different from the ϵ_r that is measured by the PWB manufacturer. Typically, the PWB manufacturer uses time-domain equipment such as an oscilloscope operating in the time-domain reflectometry (TDR) mode, whereas, laminate suppliers typically use frequency-domain equipment such as a network analyzer. Often a difference in the ϵ_r values obtained from these two techniques is observed and the PWB manufacturers then find themselves redesigning their PWB's because the TL's do not have the correct impedance. By developing a measurement technique that can be easily adopted and used by both laminate suppliers and PWB manufacturers, such as the one described here, a common ground for communication can be established.

Many of the time-domain techniques [10]–[17] previously developed for measuring ϵ_r use uniform coaxial air-line sample holders where the dielectric sample extends over a given length of the air line and fills the corresponding volume. These techniques are adequate for dielectrically isotropic materials but not for anisotropic materials. However, for PWB materials, errors may appear in the extracted ϵ_r unless the sample is aligned properly with respect to the applied electric field. This alignment is difficult to attain for PWB materials because PWB materials are usually too thin to be fabricated so that the sample spans the inside diameter of the air line, and at the same time, allow the electric-field-PWB orientation inside the air line to be the same as the electric-field-PWB orientation under normal use. Under normal use, the electric field of the electrical signals propagating on the PWB TL's is perpendicular to the surface. The work presented here uses planar TL's and, as with the other time-domain methods, uses a sampling oscilloscope operating in the TDR mode. Some time-domain techniques [10]–[15] attempt to obtain $\epsilon_r(f)$, where f is frequency, and thus require knowledge of the input pulse. The method described here obtains an ϵ_r that is the average over a given frequency band (to be discussed later) and, thus, does not require knowledge of the input pulse.

The proposed measurement method can be operated in two ways; one way (manually, method 1) does not require a computer controller and provides very fast measurement results and the second way (automatically, method 2) requires a computer controller and it provides a more accurate method that is also amenable to a numerical uncertainty assessment. Both methods use the same hardware and require dimensional

Manuscript received October 18, 1995; revised August 1996.

The author is with the Electricity Division, National Institute of Standards and Technology, Gaithersburg, MD 20899 USA.

Publisher Item Identifier S 1083-4400(96)09380-1.

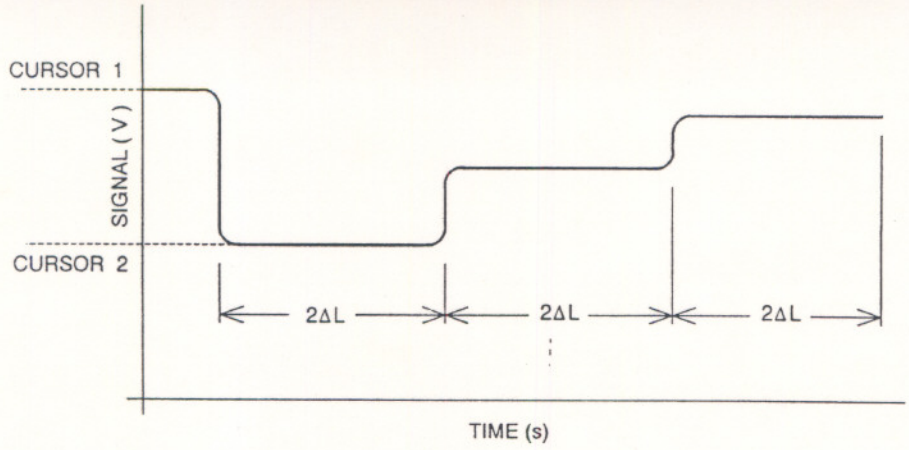

Fig. 1. Idealized TDR signal.

TABLE I
PHYSICAL DIMENSIONS OF MEASURED SAMPLES

SAMPLE	W (m) {in}	t_T (m) {in}	t_m (m) {in}	t_d (m) {in}
S1	1.93e-2 {0.756}	1.52e-3 {0.0600}	6.4e-5 {0.0025}	1.40e-3 {0.0550}
S2	1.92e-2 {0.755}	2.553e-3 {0.1005}	3.8e-5 {0.0015}	2.48e-3 {0.0975}
S3	6.12e-3 {0.241}	4.19e-4 {0.0165}	1.5e-5 {0.0006}	3.89e-4 {0.0153}
S4	3.25e-3 {0.128}	1.9e-4 {0.0073}	3.3e-5 {0.0013}	1.2e-4 {0.0047}
S5	6.43e-3 {0.253}	6.73e-4 {0.0265}	3.1e-5 {0.0012}	6.12e-4 {0.0241}
S6	5.08e-3 {0.200}	1.87e-3 {0.0735}	1.57e-3/3.8e-5 {0.0620/0.0015}	2.54e-4 {0.0100}

measurements of the TL sample. The difference between methods 1 and 2 is in the acquisition of the reflection coefficient data from which ϵ_r is extracted. Method 1 uses the oscilloscope-displayed reflection coefficient, making measurement uncertainty operator-dependent, whereas method 2 uses the computer-acquired reflection coefficient data which makes measurement uncertainty dependent on measurement noise.

II. EXPERIMENTAL

The measurement system used to acquire ϵ_r for PWB dielectrics requires an equivalent-time (nominally 50-Ω input impedance) sampling oscilloscope and a computer controller to obtain reflection coefficient data from which ϵ_r is extracted. The sampling oscilloscope makes use of the built-in pulse generator and is operated in the TDR mode. In the TDR mode, the oscilloscope delivers a rectangular voltage pulse to the sample and then records the pulse that is reflected from the sample. The reflected pulse is a consequence of the impedance discontinuity between the oscilloscope and the sample and, therefore, provides a measurement of the sample's impedance from which ϵ_r is extracted. The TDR signal that we observed is represented by the trace shown in Fig. 1. The duration of the steps in Fig. 1 corresponds to the round trip propagation time of the TL. The amplitude of the steps reflects the impedance discontinuities between the TL and the oscilloscope and between the TL and its termination. Here, the termination is an open circuit and we use only the first reflected step.

The sample uses a parallel-plate transmission line (PPTL) structure to minimize design and fabrication complexity. Sample preparation for the PPTL is extremely simple. A TL of length, L, having a uniform width, W, is sheared from a sheet of laminate. Both sides of the laminate must be metal clad. The sample should be prepared so that the long edges of the PPTL are as parallel as possible. Deviations from parallel increase measurement uncertainty as explained in Appendix A. The edges should be deburred to ensure that the electric field is uniform along the length of the samples. The widths of the samples were initially chosen arbitrarily (see Tables I and II); however, an analysis later showed that an optimal TL impedance may be around 14 Ω (see Appendix B). This result has not yet been experimentally tested or verified. All samples prepared subsequent to those of Tables I and II were made to have an approximate impedance of 14 Ω. The sample holder used is a coaxial-to-stripline adapter (see Fig. 2). The sample is placed between the center conductor and two of the four ground tabs of the adapter.

TABLE II
EXTRACTED DIELECTRIC CONSTANT AND MODEL PARAMETERS. THE $[\epsilon_{r,\mathrm{eff}}^{\mathrm{refl}}]$ IS EXPLAINED IN THE TEXT

SAMPLE	ρ	Z_T (Ω)	$Z_{PL,air}$ (Ω)	$Z_{PL,s}$ (Ω)	$Z_{PP,s}$ (Ω)	ϵ_r {target} $[\epsilon_{r,\mathrm{eff}}^{\mathrm{refl}}]$
S1	-0.612	12.04	459.4	219.4	13.1	4.382 {4.384[1]} [5.19]
S2	-0.580	13.29	585.9	177.3	14.73	10.92 {10.8 ± 0.25[11]} [13.42]
S3	-0.630	11.35	476.4	243.1	12.21	3.841 {3.91[1]} [4.45]
S4	-0.762	6.754	265.3	139.8	7.292	3.604 {3.58[1]} [4.20]
S5	-0.650	10.61	448.9	146.7	11.73	9.37 {10.2 ± 0.5[12]} [11.46]
S6	-0.800	5.56	342.3	108.2	5.96	10.01 {10.8 ± 0.25[11]} [11.49]

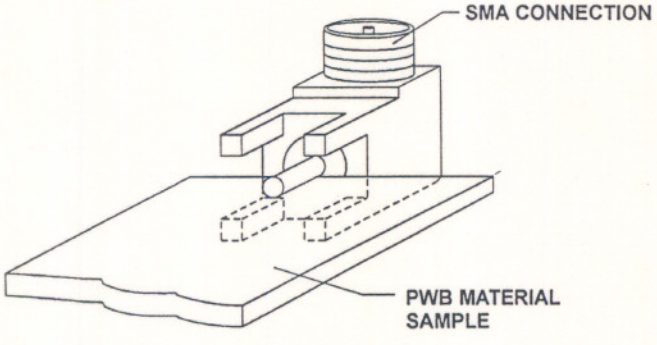

Fig. 2. Schematic of PWB right-angle jack that was used as the sample holder.

The ϵ_r of the sample material is extracted from the PPTL impedance which in turn is obtained from the observed reflection coefficient, ρ

$$\rho = \frac{Z_T - Z_0}{Z_T + Z_0} \tag{1}$$

and, therefore

$$Z_T = Z_0 \frac{1+\rho}{1-\rho} \tag{2}$$

where Z_T and Z_0 are the PPTL and the oscilloscope impedances and are real-valued in this case. In method 1, ρ is obtained from the oscilloscope display and is the difference between the vertical positions of the horizontal-line cursors that are placed colinearly along the nominally flat regions of the TDR signal (see Fig. 1). For method 2, ρ is acquired using the computer and is averaged over the time corresponding to the round trip pulse propagation time. The corresponding value for ϵ_r is then extracted from ρ using (1), (2), and (8). The ϵ_r found with this technique is the average over the frequency range of the measurement. The lower limit of this range is dependent on the duration of the displayed TDR signal. For example, an observation time of 10 ns corresponds to a lower limit of 1/10 ns or 100 MHz. The upper limit is based on the approximation $f = 0.35/t_{\mathrm{fall}}$, where t_{fall} is the observed 90%–10% transition of the PPTL-induced reflected pulse and f is frequency. So, for a 10 ns window and $t_{\mathrm{fall}} \approx 70$ ps, the bandwidth is 0.1 GHz to 5 GHz: this is what is assumed here.

III. SIMULATIONS AND MODEL

To obtain an estimate for ϵ_r, the electrical behavior of the TL must be modeled correctly. To do this, simulations of PPTL's having various geometries (widths and dielectric thicknesses) and various ϵ_r values were performed and the characteristics of the PPTL's studied. Measurements using the PPTL configuration were then performed on materials having a known ϵ_r. However, the measurements did not agree with the expected results of the simulations; the measurement data yielded higher-than-actual ϵ_r values. A possible explanation for this discrepancy is that the model used in the simulation described an ideal PPTL immersed in a material of ϵ_r, whereas in the actual PPTL, the ϵ_r between the conductors is different from that of the surrounding environment, namely air. Consequently, there is an effective dielectric value that affects the line impedance and, therefore, the extraction of an accurate ϵ_r. To check this hypothesis, PPTL samples having various widths were obtained from a common sheet of material and ϵ_r extracted from ρ measurements. The results (not shown in this paper) clearly indicated a dependence of ϵ_r on the PPTL width, W. A possible model for the PPTL samples which could explain the observed behavior is that the actual PPTL behaves as if it were three ideal transmission lines in parallel (see Fig. 3): an ideal PPTL having an impedance $Z_{\mathrm{PP},s}$, an ideal parallel line transmission line (PLTL) immersed in an air dielectric with impedance $Z_{\mathrm{PL,air}}$, and an ideal PLTL immersed in the sample material having an impedance $Z_{\mathrm{PL},s}$. Therefore, the total impedance of the actual PPTL, Z_T, can

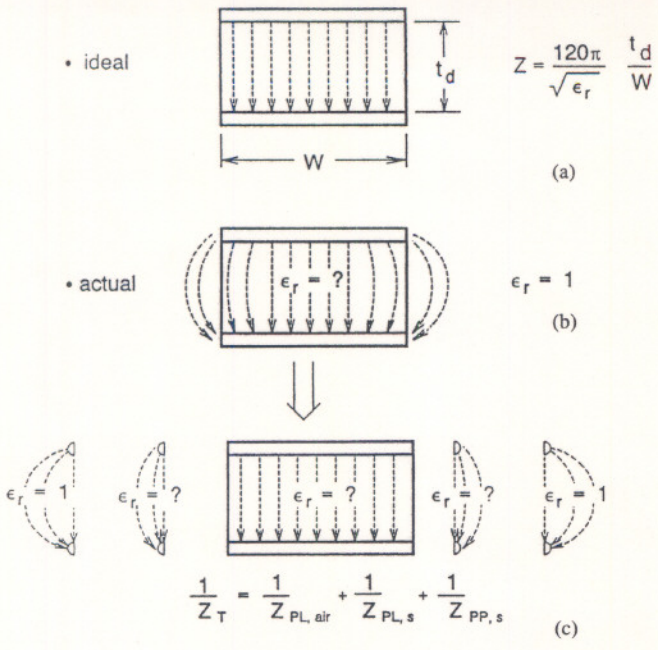

Fig. 3. Electric field pattern for parallel-plate transmission line: (a) ideal, (b) actual, and (c) modeled.

be described by

$$\frac{1}{Z_T} = \frac{1}{Z_{\mathrm{PL,air}}} + \frac{1}{Z_{\mathrm{PL},s}} + \frac{1}{Z_{\mathrm{PP},s}} \tag{3}$$

where $Z_{\mathrm{PL,air}}$ is given by [18]

$$Z_{\mathrm{PL,air}} = 120 \cosh^{-1}\left(\frac{s}{t_m}\right) \tag{4}$$

and t_m is the thickness of the conductors and s is the center-to-center spacing between conductors; $Z_{\mathrm{PL},s}$ is given by [18]

$$Z_{\mathrm{PL},s} = \frac{Z_{\mathrm{PL,air}}}{\sqrt{\epsilon_r}} \tag{5}$$

and $Z_{\mathrm{PP},s}$ is given by [18]

$$Z_{\mathrm{PP},s} = \frac{120\pi}{\sqrt{\epsilon_r}} \frac{t_d}{W}. \tag{6}$$

The two variables s and t_d are most easily obtained not from direct measurements but from measurements of t_m and the total sample thickness, t_T.

The t_m should be inferred from the "weight" and density of the copper cladding; this is discussed

$$\begin{aligned} s &= t_T - t_m \\ t_d &= t_T - 2t_m \end{aligned} \tag{7}$$

further in the Section VI.

The model predicts that the reciprocal impedance as a function of line width will have a nonzero line-width intercept and a slope proportional to the square root of ϵ_r. Four samples having different widths were prepared and the reciprocal impedance as a function of line width was calculated from the data for these samples and plotted (see Fig. 4). The data agree well with a fit to the model.

IV. Results

A. Method 1

Various PPTL samples were prepared and measured and values for ϵ_r extracted using this method. It is important to note that the ϵ_r values obtained and presented here required only one PPTL sample for each different material and that the multiple samples of different widths were solely for model verification. The physical dimensions of the PPTL samples are given in Table I. Combining (3)–(7) and solving for ϵ_r gives

$$\epsilon_r = \left(\frac{\left[120 \cosh^{-1}\left(\frac{t_T - t_m}{t_m}\right) - Z_T\right]\pi(t_T - 2t_m)}{Z_T\left[\pi(t_T - 2t_m) + W \cosh^{-1}\left(\frac{t_T - t_m}{t_m}\right)\right]} \right)^2. \tag{8}$$

The ϵ_r values extracted from the measured reflection-coefficient data using (8) are shown in Table II along with nominal target values where the target values are either manufacturer's specifications or the results of resonant-cavity methods performed by the Electromagnetic Fields Division at NIST, Boulder, CO. The $\epsilon_{r,\mathrm{eff}}^{\mathrm{refl}}$ value, which is the dielectric constant calculated using the assumption that the PPTL is an ideal line is also shown in Table II. The $\epsilon_{r,\mathrm{eff}}^{\mathrm{refl}}$ provides an upper limit for ϵ_r and it also shows that the time-domain data can give an erroneous reading if the proper TL model is not used. The last two ϵ_r entries in Table II show a significant deviation from the target values compared to the other four entries. For the next-to-the-last entry this may be due to a line-length effect: the corresponding PPTL was much shorter than the other PPTL's, approximately 7.6 cm (3″) long compared to 20.3 cm or 22.9 cm (8″ or 9″) long. To determine if line length did indeed affect the measurement, FR4 samples of various lengths were prepared and examined. Table III shows the result for two different widths, 1.9 cm (3/4″) and 1.3 cm (1/2″). This line-length effect is a low-frequency effect and may be caused by the length-dependent low-frequency electrical load of the PPTL. Consequently, line lengths should exceed 25.4 cm (10″) to avoid this potential source of error. The sample corresponding to the last entry had a thick conductor on one side (see Table I) that caused the dielectric to partially delaminate during sample preparation which may have caused the deviation from the target value. In general, however, the results in Table II, corresponding to method 1, indicate excellent agreement between target values and those obtained by this measurement method.

B. Method 2

Several new samples were prepared for analysis using the more accurate process of this method. The ϵ_r results, along with uncertainties, are shown in Table IV. More will be said about uncertainties in the next section. Samples S8 through S11 show a continuous increase in the extracted ϵ_r with increasing number of plies. This may be due to an unexpected thickness-dependence on the measurement results or to the construction of the PWB itself: the variation in actual ϵ_r of the PWB material may be caused by the interface between

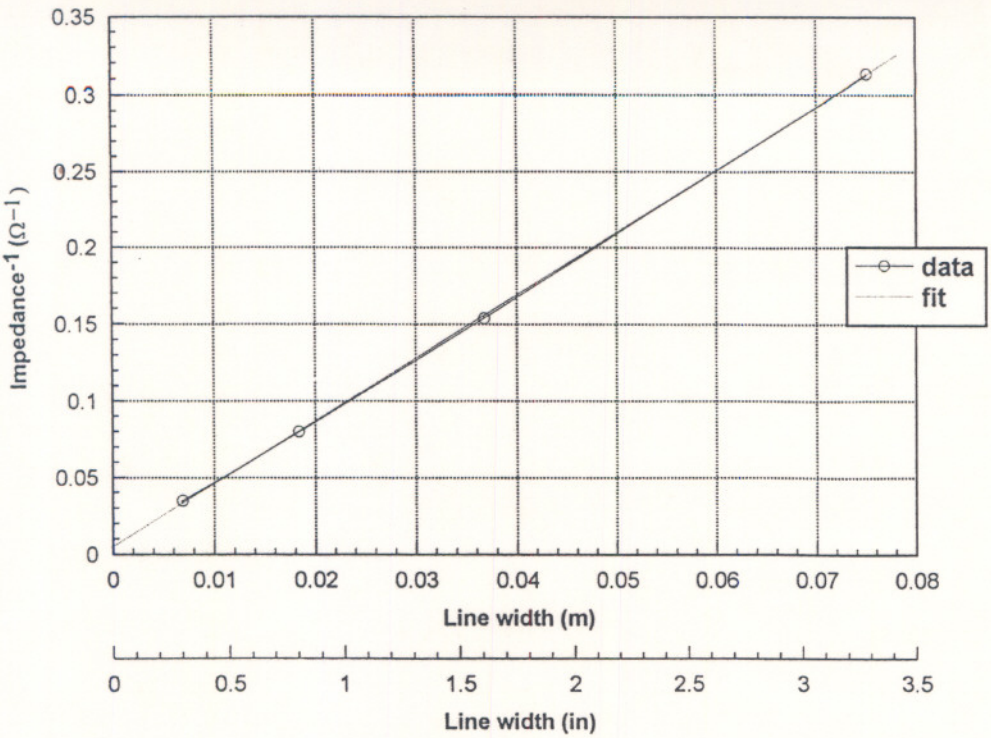

Fig. 4. Reciprocal impedance plotted as function of line width. The solid line represents measured data (the circles represent the actual data values) and the dashed line is a linear fit extrapolated to $W = 0$.

TABLE III
OBSERVED REFLECTION COEFFICIENT, ρ, FOR VARIOUS LENGTHS OF 0.019 m (3/4″ WIDE AND 0.025 m (1″) WIDE FR4 PPTL SAMPLES

L (m) (in)	0.51 {20}	0.38 {15}	0.30 {12}	0.25 {10}	0.23 {9}	0.18 {7}	0.15 {6}	0.10 {4}	0.08 {3}
ρ 0.019 m (3/4")	-0.610	-0.610	-0.610	-0.610	-0.610	--	--	-0.600	--
ρ 0.025 m (1")	--	--	-0.680	--	-0.680	-0.680	-0.670	--	-0.660

plies or by a variation of ϵ_r between plies. Consequently, it may be difficult to ascertain if the ply-dependent ϵ_r for S8–S11 in Table IV are a measurement artifact or real. It may also be difficult to determine what causes the thickness-dependence for single-ply boards of the same material because material properties vary between production runs and single plies having different thicknesses require different production runs. Sample S7 deviates significantly from the S8–S11 trend probably because S7 was very narrow, about 800-μm wide, and any imperfections in the shear blade could have significant effects on ρ. A large perturbation was observed in the TDR signal that correlated with a notch in the sample width. Other wider samples also had similar notches but they did not display the effect as greatly as S7. Furthermore, the metal roughness may affect measurement accuracy. Preparing the samples by routing instead of shearing may reduce the calculated measurement uncertainty because the edges would be more uniform and parallel in routed samples than in sheared samples.

During measurements using a reference short-circuit, it was noticed that the short-circuit reflection coefficient was not equal to -1 and that an offset error was present. Accordingly, reflection coefficients obtained should be corrected for these two errors

$$\rho' = \frac{\rho - \rho_{\text{off}}}{\rho_{\text{off}} - \rho_{sc}}. \tag{9}$$

All subsequent ρ measurements must be corrected according to (9) and the impedance, Z_T, of the PPTL found relative to Z_0

$$Z_T = Z_0\left(\frac{1+\rho'}{1-\rho'}\right). \tag{10}$$

V. ERROR AND UNCERTAINTY ANALYSIS

An error and uncertainty analysis is performed here to determine to which measurable parameters the calculation of ϵ_r is sensitive. The general equation for the propagation of uncertainties, assuming the measurement uncertainties of the parameters is independent of and uncorrelated to each other and that the uncertainties are normally distributed and

TABLE IV
MEASURED PHYSICAL PARAMETERS, OBSERVED REFLECTION COEFFICIENT, AND EXTRACTED ϵ_r

SAMPLE	reflection coefficient, ρ	total thickness, t_T (m)	metal thickness, t_m (m)	width, W (m)	ϵ_r {target}
S7 (1 ply)	-5.174e-1 ± 1.42e-2	1.6586e-4	3.43e-5 ± 3.43e-6	8.1255e-4	5.412 ± 1.47 {4.11‡2}
S8 (2 ply)	-5.025e-1 ± 8.46e-3	2.0371e-4	3.43e-5 ± 3.43e-6	1.4790e-3	3.261 ± 0.696 {4.11‡2}
S9 (4 ply)	-5.626e-1 ± 5.79e-3	3.2182e-4	3.43e-5 ± 3.43e-6	3.2286e-3	3.753 ± 0.524 {4.11‡2}
S10 (8 ply)	-5.654e-1 ± 9.51e-3	5.9055e-4	3.43e-5 ± 3.43e-6	6.8153e-3	3.825 ± 0.410 {4.11‡2}
S11 (16 ply)	-5.678e-1 ± 1.25e-2	1.0950e-3	3.43e-5 ± 3.43e-6	1.3515e-2	3.940 ± 0.401 {4.11‡2}
S12	-5.705e-1 ± 9.03e-3	1.5305e-3	1.72e-5 ± 1.72e-6	1.9204e-2	4.348 ± 0.322
S13	-5.676e-1 ± 5.01e-3	1.4831e-3	1.72e-5 ± 1.72e-6	1.8964e-2	4.111 ± 0.240
S14	-5.907e-1 ± 8.55e-3	1.5127e-3	6.86e-5 ± 6.86e-6	1.8868e-2	4.318 ± 0.395 {4.384†}
S15	-5.833e-1 ± 1.12e-2	1.3404e-3	3.43e-5 ± 3.43e-6	1.0641e-2	10.20 ± 0.953 {10.2‡1}
S16	-5.595e-1 ± 1.12e-2	1.3802e-3	3.43e-5 ± 3.43e-6	1.3467e-2	6.040 ± 0.551 {6.15‡1}
S17	-6.049e-1 ± 1.48e-2	7.9451e-4	3.43e-5 ± 3.43e-6	1.4130e-2	2.335 ± 0.290 {2.2‡1}

† Measured values obtained by NIST-Boulder, measured at 16 GHz.
‡1 Manufacturer specification, measured at 10 GHz.
‡2 Manufacturer specification, measured at 1 MHz.

expressed in the same number of standard deviations is [19]

$$u_T = \sqrt{\sum_{i=1}^{M} \left(\frac{\partial f}{\partial x_i}\right)^2 u_i^2} \tag{11}$$

where x_i are the measurement variables, u_i are the uncertainties associated with the x_i, and u_T is the total measurement uncertainty. The variables are W, t_T, t_m, Z_0, and ρ; ρ_{sc} is the the short-circuit reflection coefficient and ρ_{off} is the reflection-coefficient offset error. Because the partial derivatives of ϵ_r with respect to $W, t_T, t_m, Z_0, \rho, \rho_{sc}$, and ρ_{off} are rather lengthy, these are given in Appendix C.

The measurement uncertainties presented here represent either one or three standard deviations (1σ for method 1 and 3σ for method 2). Table V shows the 1s ϵ_r uncertainties, u_{T1}, using method 1 (samples from Tables I and II). In addition, the squares of the values of the partial derivatives used to calculate u_{T1} are shown in Table V. The 1σ-uncertainties in W, t_T, t_m, Z_0, and ρ for the data in Table V are $\pm 5.04 \times 10^{-4}$ m $(0.02'')$, $\pm 1.27 \times 10^{-5}$ m $(0.0005'')$, $\pm 1.27 \times 10^{-5}$ m $(0.0005'')$, $\pm 0.167\,\Omega$, and ± 0.006. Table V also shows the importance of having small dimensional uncertainties and an accurately-known reference impedance, Z_0. However, obtaining less than $\pm 1\%$ 3σ-uncertainty in Z_0 is difficult.

Table VI displays the uncertainties in the values of ϵ_r extracted by method 2, u_{T2}, and the possible contributors to u_{T2}. For the data presented in Tables IV and VI, the values used for Z_0, ρ_{sc}, and ρ_{off} and their associated 3σ-uncertainties were $Z_0 = 50 \pm 0.5\,\Omega, \rho_{sc} = -0.994 \pm 3.36 \times 10^{-3}$, and $\rho_{\text{off}} = 2.2094 \times 10^{-2} \pm 1.37 \times 10^{-3}$. The 3σ uncertainties for W and t_T were 2.45e-6 m $(0.0001'')$ and for t_m was 10% of t_m. All uncertainties shown in Tables IV and VI are 3σ uncertainties. From Table VI, it is easy to see that the largest uncertainty contributors are ρ and t_m.

The calculated uncertainties, u_{T2}, are much greater than the variations in ϵ_r extracted from different samples. For example, six additional samples were sheared from the same sheet from which S11 was obtained and then the average extracted ϵ_r from these six samples was calculated. The average extracted ϵ_r was 3.953 and had a 3σ variation of 0.093. This 3σ variation is about four times less than the u_{T2} of 0.401 for S11.

The uncertainty in ρ reflects measurement noise and variations in the physical dimensions of the PPTL, that is, of $W(x), t_T(x)$, and $t_m(x)$, where x is position along the PPTL. Recall, that the ρ used is an average for the PPTL sample and, therefore, variations in $W(x), t_T(x)$, and $t_m(x)$ contribute to uncertainties in ρ. The variables W, t_T, and t_m are, for this analysis, the average values of $W(x), t_T(x)$, and $t_m(x)$ over the sample length. What is important here are the uncertainties of these average values (see Appendix A), which is found by obtaining many average values and then finding the average and standard deviation of that group of averages. The actual measurement uncertainties of $W(x), t_T(x)$, and $t_m(x)$ can be much less than their variations along a given PPTL. For example, by using an accurate digital micrometer, the 3σ uncertainty in the measurements of $W(x)$ and $t_T(x)$ can be reduced to about ± 2.54e-6 m $(0.0001'')$. The variations in $t_T(x)$ and $t_m(x)$ are fixed by the manufacturing process and cannot be controlled here. However, variations in $W(x)$ can

TABLE V
MEASUREMENT UNCERTAINITES FOR METHOD 1. THE VALUES IN CURLY BRACKETS ARE THE SQUARES OF THE VALUES OF THE PARTIAL DERIVATIVES THAT ARE USED IN THE UNCERTAINTY ANALYSIS [SEE (11)]. ALL UNCERTAINTIES REPRESENT ONE STANDARD DEVIATION

SAMPLE	$(\partial\epsilon_r/\partial W)^2$ (m^{-2}) $\{in^{-2}\}$ $[u_W \lvert \partial\epsilon_r/\partial W \rvert]$	$(\partial\epsilon_r/\partial t_T)^2$ (m^{-2}) $\{in^{-2}\}$ $[u_{t_T} \lvert \partial\epsilon_r/\partial t_T \rvert]$	$(\partial\epsilon_r/\partial t_m)^2$ (m^{-2}) $\{in^{-2}\}$ $[u_{t_m} \lvert \partial\epsilon_r/\partial t_m \rvert]$	$(\partial\epsilon_r/Z_0)^2$ (Ω^{-2}) $[u_{Z_0} \lvert \partial\epsilon_r/Z_0 \rvert]$	$(\partial\epsilon_r/\rho)^2$ $[u_\rho \lvert \partial\epsilon_r/\rho \rvert]$	u_{T1}
S1	1.81e5 {1.17e2} [2.16e-1]	3.63e7 {2.34e4} [7.65e-2]	2.21e8 {1.43e5} [1.89e-1]	3.21e-2 [2.99e-2]	8.14e2 [1.71e-1]	0.344
S2	1.10e6 {7.10e2} [5.33e-1]	6.92e7 {4.46e4} [1.06e-1]	7.94e8 {5.12e5} [3.58e-1]	1.99e-1 [7.43e-2]	4.52e3 [4.04e-1]	0.770
S3	1.43e6 {9.23e2} [6.07e-1]	3.68e8 {2.37e5} [2.44e-1]	2.24e9 {1.45e6} [6.01e-1]	2.50e-2 [2.64e-2]	6.83e2 [1.57e-1]	0.903
S4	4.78e6 {3.08e3} [1.11]	3.48e9 {2.25e6} [7.49e-1]	1.54e10 {9.94e6} [1.57]	2.40e-2 [2.58e-2]	1.34e3 [2.20e-1]	2.08
S5	7.24e6 {4.67e3} [1.37]	8.46e9 {5.46e6} [1.17]	5.38e9 {3.47e6} [9.32e-1]	1.46e-1 [6.37e-2]	4.39e3 [4.21e-1]	2.07
S6	3.65e8 {2.35e5} [9.70]	3.26e9 {2.10e6} [7.25e-1]	6.46e10 {4.17e7} [3.24]	5.94 [4.06e-1]	4.58e5 [4.18]	11.1
average (excluding S6)	2.95e6 {1.90e3} [7.67e-1]	2.48e9 {1.60e6} [6.14e-1]	4.81e9 {3.10e6} [7.30e-1]	8.52e-2 [4.86e-2]	2.35e3 [2.75e-1]	1.03

TABLE VI
MEASUREMENT UNCERTAINTIES FOR MEASUREMENT TECHNIQUE METHOD 2. ALL UNCERTAINTIES REPRESENT THREE STANDARD DEVIATIONS

SAMPLE	from ρ	from ρ_{sc}	from ρ_{off}	from t_T	from t_m	from W	from Z_0	u_{T2}
S7 (1 ply)	4.50e-1	5.65e-2	2.04e-2	1.40e-1	1.38	2.75e-2	1.16e-1	1.47
S8 (2 ply)	1.57e-1	3.22e-2	1.23e-2	9.60e-3	6.64e-1	7.83e-2	6.93e-2	6.90e-1
S9 (4 ply)	1.23e-1	4.44e-2	1.34e-2	5.33e-2	4.96e-1	5.23e-3	7.82e-2	5.24e-1
S10 (8 ply)	2.23e-1	4.54e-2	1.35e-2	3.38e-2	3.31e-1	2.57e-3	7.90e-2	4.10e-1
S11 (16 ply)	3.01e-1	4.68e-2	1.38e-2	2.23e-2	2.47e-1	1.39e-3	8.10e-2	4.01e-1
S12	2.39e-1	5.19e-2	1.51e-2	2.44e-2	1.87e-1	1.06e-3	8.88e-2	3.22e-1
S13	1.25e-1	4.86e-2	1.43e-2	2.36e-2	1.78e-1	1.01e-3	8.40e-2	2.40e-1
S14	2.25e-1	5.33e-2	1.43e-2	1.52e-2	3.08e-1	1.01e-3	8.51e-2	3.93e-1
S15	7.14e-1	1.28e-1	3.53e-2	4.92e-2	5.79e-1	4.32e-3	2.09e-1	9.53e-1
S16	4.07e-1	6.98e-2	2.13e-2	2.89e-2	3.41e-1	2.05e-3	1.24e-1	5.51e-1
S17	2.26e-1	3.16e-2	7.80e-3	1.68e-2	1.71e-1	7.77e-4	4.79e-2	2.90e-1
average	2.91e-1	5.53e-2	1.65e-2	3.79e-2	4.44e-1	1.14e-2	9.66e-2	5.68e-1

be reduced by careful attention to sample preparation. By reducing $W(x)$-variations, the uncertainty in ρ can also be reduced (see Appendix A).

As mentioned earlier, one can use the "weight" (weight per unit area, typically given in ounces per square foot, is implied) of the conductor to infer its thickness. According to the Institute for Interconnecting and Packaging Electronic Circuits (IPC) specification ANSI/IPC-MF-150F, the variation in conductor thickness is less than $\pm 5\%$ for wrought copper foils and less than $\pm 10\%$ for electrodeposited copper foils and the density of copper is 8.93 gr/cm^3 $\pm 1\%$. The percent thickness variation in the t_m measured for samples S1–S6 ranges from 20% (sample S1) to 83% (sample S3). Consequently, the t_m uncertainty contribution, assuming adherence of the metal foil manufacturer to ANSI/IPC-MF-150F, can be significantly reduced by using the manufacturers' specifications and ANSI/IPC-MF-150F. This assumption was used in the data presented in Table VI. In practice, it is better to use ANSI/IPC-MF-150F for t_m and then subtract this from t_T to get t_d than it is to measure t_d directly. Not only does the ANSI/IPC specification give smaller variations than can be measured simply, but the effects of the roughness of the copper foil can be ignored. The copper surface is roughened to enhance adhesion between the copper and the dielectric.

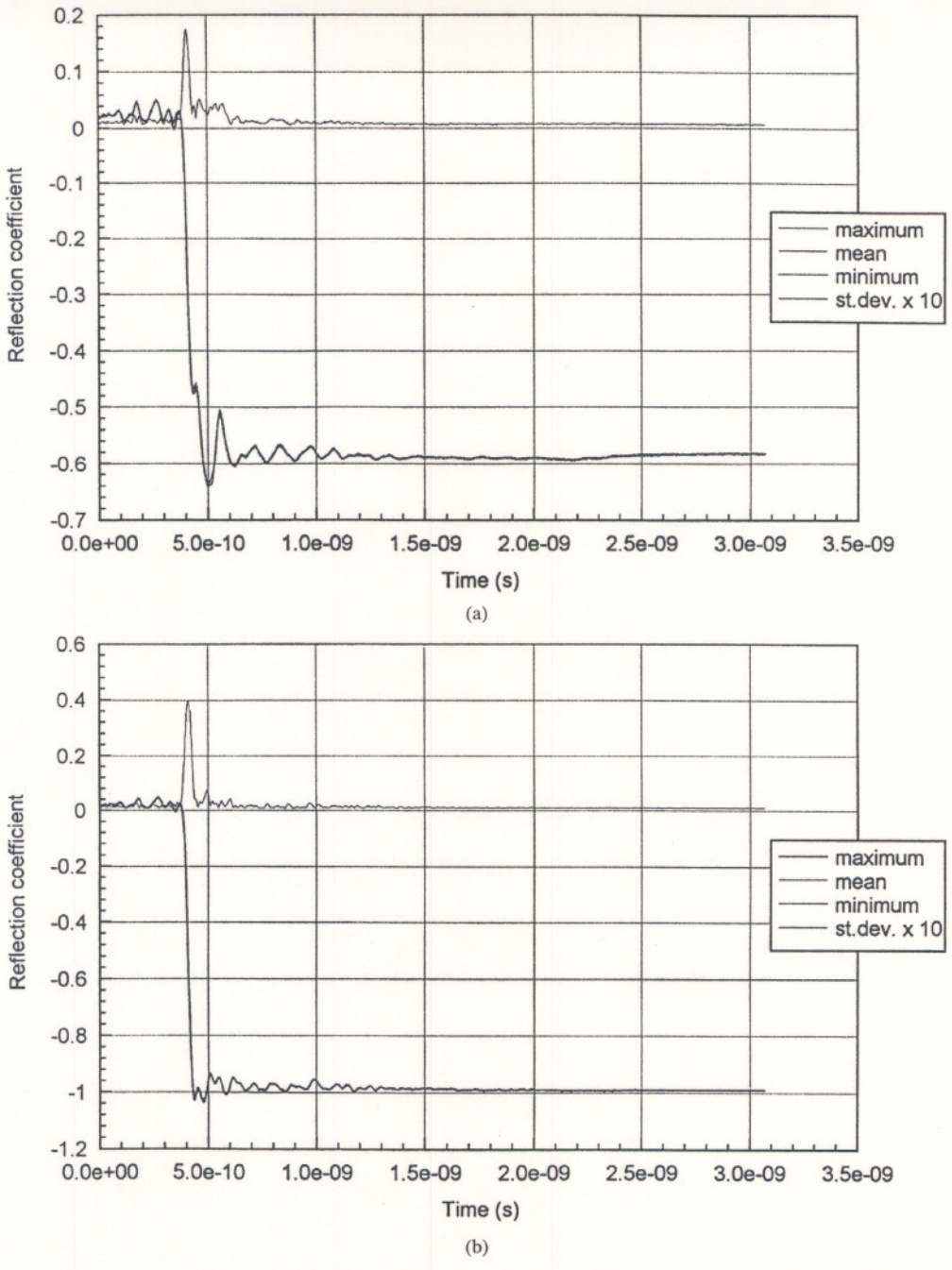

Fig. 5. Reflection-coefficient traces corresponding to the maximum, mean, minimum, and standard deviation for the (a) sample and (b) reference measurements. Ten measurements each for both the reference and sample were taken.

This roughened surface, however, creates a mirror image on the dielectric surface so that a direct measure of the dielectric thickness will give a peak-to-peak value. Using ANSI/IPC-MF-150F, we will not be subject to this peak-to-peak error because the outer surface of the copper foils is relatively smooth. Furthermore, ANSI/IPC-MF-150F for t_m is based on the mass of the copper so that t_m based on ANSI/IPC-MF-150F is a mean value. Consequently, $t_T - 2t_m$ will result in a more accurate estimate of the mean value of the dielectric thickness than that obtained from a direct measurement.

Errors in the measurement of ρ can arise from two other sources: lack of repeatability of sample insertion and the position of the sample-holder center pin with respect to sample center. The repeatability issue was examined by taking ten consecutive data sets, where a set consists of a reference (short-circuit) and a sample measurement, and comparing the reference and sample data. In particular, the data were taken so that the transition between the 50-Ω oscilloscope impedance and sample impedance could be observed. The appearance of this transition region is the most sensitive to sample insertion. The mean, maximum, minimum, and standard deviation as a function of time for both the ten reference and ten sample measurements were calculated. The results are shown in Fig. 5. The peaks in the standard deviation curves are caused primarily by time-base drift and not sample insertion repeatability. This is supported by the independent

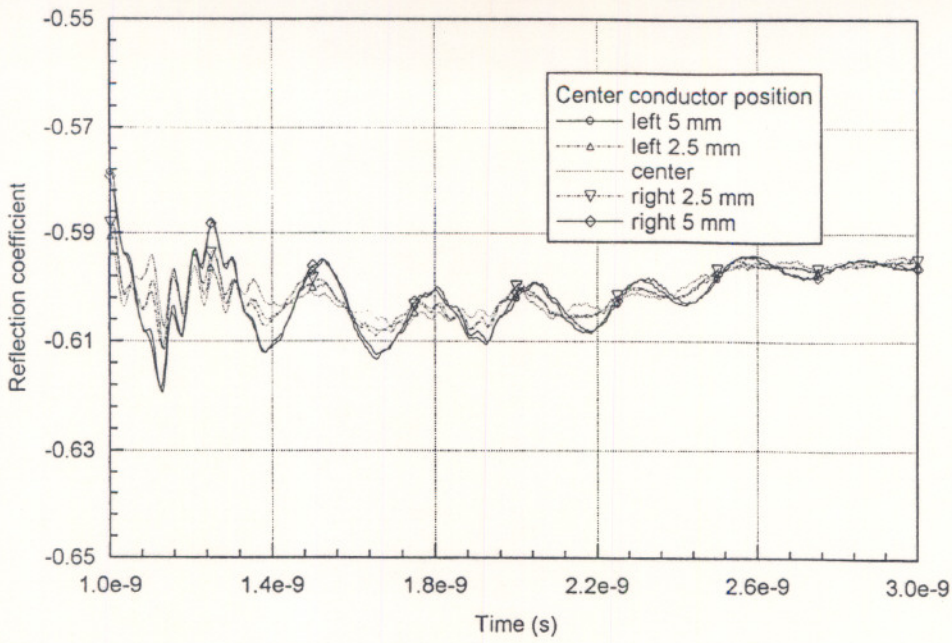

Fig. 6. Reflection-coefficient traces corresponding to different locations of the sample-holder center pin relative to the center of the sample.

TABLE VII
MEAN AND 3σ STANDARD DEVIATION FOR THE REFLECTION COEFFICIENT BOUND BETWEEN THE 1 ns AND 3 ns TIMES IN FIG. 6. EACH VALUE CORRESPONDS TO THE POSITION OF THE SAMPLE-HOLDER CENTER PIN RELATIVE TO SAMPLE CENTER

center pin position relative to sample center	reflection coefficient
5 mm to the left	-6.0111e-1 ± 6.15e-3
2.5 mm to the left	-6.0100e-1 ± 4.20e-3
centered	-6.0074e-1 ± 3.83e-3
2.5 mm to the right	-6.0077e-1 ± 4.37e-3
5 mm to the right	-6.0136e-1 ± 6.15e-3

observation of time-base drift and by the correspondence between the peaks of the first-differences (first derivatives) of the mean curves and the peaks of the standard-deviation curves. Furthermore, the mean and 3σ standard deviation in ρ for the reference and sample sets are $-9.8987\times10^{-1}\pm3.273\times10^{-3}$ and $-5.875\,79\times10^{-1}\pm2.30\times10^{-3}$, which shows that sample insertion is a negligible contribution to measurement error.

To examine the effect of the position of the center pin on the measurement, five measurements were taken from a 19 mm wide sample where the center pin was placed at different positions relative to the center of the sample (see Fig. 6). Table VII also shows the mean and standard deviation of ρ for the region between 1 ns and 3 ns. The ρ is relatively insensitive to center pin location.

A couple of general comments can be made on comparing the uncertainties for the two measurement methods. Even though the uncertainties are much greater for method 1 than method 2, there are more uncertainty contributions in method 2 than in method 1. The uncertainty contributions in method 1 from sample width and thickness were reduced significantly by careful measurement using an accurate digital micrometer. A reduction in ρ uncertainty was attained by attention to sample preparation. And, if one can confidently assert the IPC specifications for metal-thickness uncertainty, we get a decrease in metal-thickness uncertainty by a factor of four to eight.

VI. CONCLUSION

A new measurement method, based on a simple transmission line structure, was developed to extract an average value for the permittivity in dielectric materials, ϵ_r, from a measurement of the transmission-line reflection coefficient, ρ. Sample preparation and measurement analysis for the method is simple. The method uses a sampling oscilloscope and ϵ_r can be readily extracted from the observed or acquired ρ and sample dimensions. The insensitivity to the position of the sample in the sample holder and high repeatability make this a robust measurement technique for ϵ_r. The 3σ uncertainties for the extracted ϵ_r, calculated from a propagation of uncertainties for the six parameters that can affect ϵ_r, are less than 10%. The 3σ variations in ϵ_r obtained from almost-identical samples that were prepared by shearing is about 2%. Finally, we can infer an average accuracy in the extracted ϵ_r of better than 2% by comparing the results of this work to manufacturer specifications or the results of resonant-cavity measurements.

APPENDIX A
EFFECTS OF POSITIONAL VARIATIONS OF SAMPLE WIDTH AND THICKNESS ON ϵ_r UNCERTAINTY

The reflection coefficient, ρ, used in the main part of this paper is actually the average of $\rho(x)$, where x is the direction of propagation of the pulse along the PPTL. Consequently, the uncertainty σ_ρ, contains not only uncertainty contributions from the measurement of $\rho(x)$, but also from the effects of the variations in the width and thickness of the PPTL sample along its length. This latter contribution is a consequence of the dependence of $\rho(x)$ on $t_d(x), t_m(x)$, and $W(x)$. To understand the effect of the variations of t and W on σ_ρ, let's start with a simplifying assumption that the PPTL sample is an ideal PPTL. With this assumption, we can use (2) in (6) and rearrange to solve for ϵ_r. This gives a general equation

$$\epsilon_r(x) - \sigma_{\epsilon(x)} = \left(\frac{(120\pi)[t(x) \pm \sigma_{t(x)}]}{(Z_0 + \sigma_{Z_0})(W(x) \pm \sigma_{W(x)})} \frac{1 - \rho(x) \pm \sigma'_{\rho(x)}}{1 + \rho(x) \pm \sigma'_{\rho(x)}} \right)^2 \tag{12}$$

where $t(x) = t_d(x) + 2t_m(x)$ is used for brevity and $\sigma'_{\rho(x)}$ is the uncertainty in the measurement of $\rho(x)$. Equation (12) can be simplified by assuming that the uncertainties shown in (12) are, for the measurement described herein, independent of x, that is, for example, $\sigma_{t(x)} = \sigma_t$. Furthermore, ϵ_r should not be varying within the sample and, so, should not be a function of x. If we use these assumptions and also substitute

$$\begin{aligned} t(x) &= t + \Delta t(x) \\ W(x) &= W + \Delta W(x) \\ \rho(x) &= \rho + \Delta\rho(x) \end{aligned} \tag{13}$$

into (12), we get

$$\epsilon_r \pm \sigma_\epsilon = \left(\frac{(120\pi)[t + \Delta t(x_2) \pm \sigma_t]}{(Z_0 \pm \sigma_{Z_0})(W + \Delta W(x_3) \pm \sigma_W)} \cdot \frac{1 - \rho - \Delta\rho(x_1) \pm \sigma'_\rho}{1 + \rho + \Delta\rho(x_1) \pm \sigma'_\rho} \right)^2. \tag{14}$$

The σ_t and σ_W are the uncertainties in the measurement of t and W, t and W are the mean values of $t(x)$ and $W(x)$, and x_1, x_2, and x_3 indicate positions along the x-direction of the PPTL. The x-position correspondence between $\rho(x_1)$ and $t(x_2)$ and $W(x_3)$ is lost with this method because that positional information is not stored, only an average value of these variables over x is retained. If the x-correspondence was retained, however, the effects of variations in $W(x_3)$ and $t(x_2), \Delta W(x_3)$ and $\Delta t(x_2)$, could have been mapped to an equivalent variation in $\rho(x_1)$. Because the correlation between $\Delta W(x_3)$ and $\Delta t(x_2)$ and position is lost, $\Delta W(x_3)$ and $\Delta t(x_2)$ effectively increase the uncertainty in $\rho(x_1)$. Similarly the positional correspondence of $\Delta\rho(x_1)$ is lost. Consequently, $\Delta\rho(x_1)$ affects the uncertainty in the mean value of $\rho(x)$. Therefore, by losing the x-position correspondences between $\rho(x), W(x)$, and $t(x)$, the uncertainty in the observed ρ and the extracted ϵ_r is increased. Accordingly, (14) can be rewritten as

$$\epsilon_r \pm \sigma_\epsilon = \left(\frac{(120\pi)[t \pm \sigma_t]}{(Z_0 + \sigma_{Z_0})(W \pm \sigma_W)} \frac{1 - \rho + \sigma_\rho}{1 + \rho \pm \sigma_\rho} \right)^2 \tag{15}$$

where σ_ρ includes contributions from σ'_ρ and from the uncertainties in ρ that are caused by the unassociated x-dependent variations in t and W. The σ_t and σ_W are determined by calculating the standard deviation for a set of mean values of t and W.

APPENDIX B
OPTIMAL PPTL IMPEDANCE

What we wish to determine here is whether there exists an optimal impedance for which spurious variations in the width, W, of the PPTL sample will have a minimal effect on the observed reflection coefficient, ρ. Additionally, we must be aware of the resolution limitations presented by the oscilloscope. The width, W, is the only adjustable parameter of the sample geometry once a laminate is made and, so, W will be used to adjust the sample impedance. We will assume here that the PPTL sample is ideal and can be described by (6) and that the variations in the sample width, ΔW, are independent of W. The ΔW is caused by the sample preparation procedure. The ΔW will affect the sample impedance, $Z_{\mathrm{PP},s}$, less as W increases. Concurrently, the ΔW-induced uncertainty in the extracted ϵ_r will decrease as W increases. The ideal situation, then, is when $W \to \infty$. However, the resolution in the measurement of ρ is limited and this resolution limit restricts the maximum W. For example, if samples of widths W_1 and W_2 happen to yield the same ρ, then we will have a problem in extracting an accurate ϵ_r. Furthermore, ρ should be maximally sensitive to changes in $Z_{\mathrm{PP},s}$ to ensure measurement accuracy. Consequently, we have two opposing criteria for an optimal impedance. First, it is desirable that $W \to \infty$, or $Z_{\mathrm{PP},s} \to 0$, so that the effects of ΔW on ϵ_r uncertainty are reduced, and second, the measurement accuracy and resolution restrict how small the PPTL impedance may be.

The sensitivity of ρ with respect to variations in the PPTL impedance can be examined by considering how the variations in ρ are affected by incremental changes in PPTL impedance

$$\Delta\rho = \frac{Z + \xi Z - Z_0}{Z + \xi Z + Z_0} - \frac{Z - Z_0}{Z + Z_0} \tag{16}$$

where ξ is the incremental change of the PPTL impedance and, for brevity, Z is used for the nominal PPTL impedance. The optimal impedance for this criterion occurs when the magnitude of $\Delta\rho$ is as large as possible and, if possible, when (16) is also constant with impedance. This criterion can be considered the maximum-sensitivity-to-ΔZ criterion and, for a 50 Ω measurement system (the oscilloscope), will occur around 45 Ω. The partial derivative of $\Delta\rho$ with respect to Z and ξ

$$\frac{\partial^2 \Delta\rho}{\partial Z \partial \xi} = -2Z_0 \frac{Z + \xi Z - Z_0}{(Z + \xi Z + Z_0)^3} \Omega^{-1} \tag{17}$$

goes to zero around 45 Ω and we will use this partial derivative in the definition of the optimal impedance.

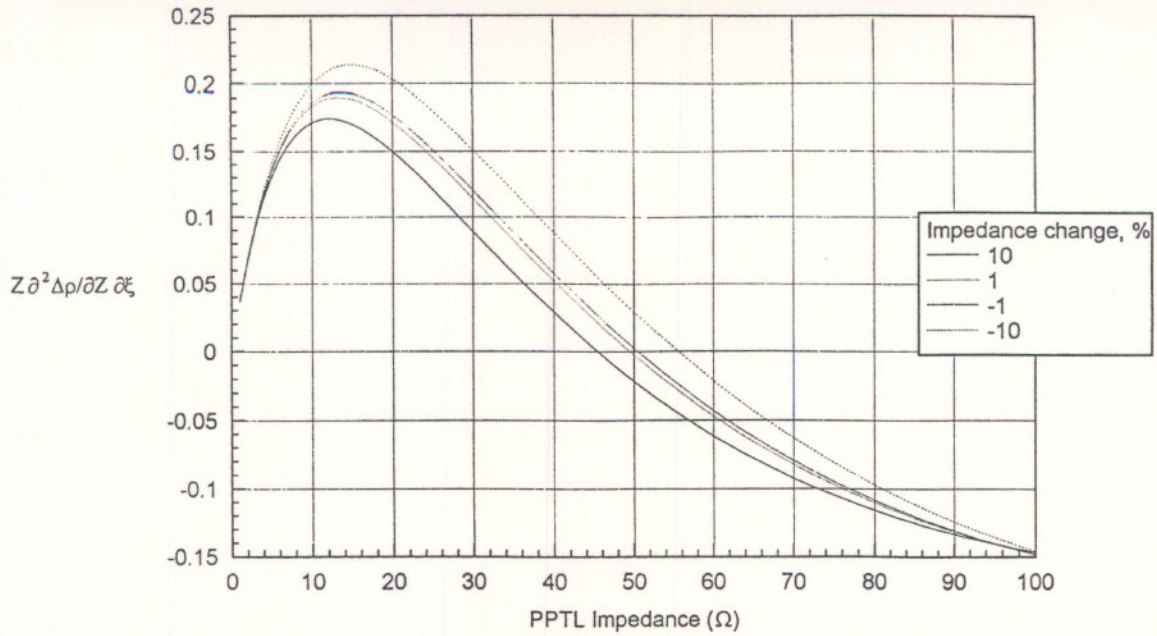

Fig. 7. A plot of $Z\partial^2\Delta\rho/\partial Z\partial\xi$ as a function of Z for impedance changes of $\pm 1\%$ and $\pm 10\%$.

To utilize both criteria, the author will define the optimal impedance as the one at which the product of (17) and Z, namely

$$Z\frac{\partial^2\Delta\rho}{\partial Z\partial\xi} = -2ZZ_0\frac{Z+\xi Z-Z_0}{(Z+\xi Z+Z_0)^3} \tag{18}$$

which is dimensionless, exhibits a maximum. This maximum occurs between 10 Ω and 16 Ω, depending on ξ. This maximum lies between the maximum-sensitivity-to-ΔZ criterion (which occurs around 45 Ω) and the minimum-sensitivity-to-ΔW criterion (which occurs at 0 Ω). Plots of (18) for $\xi = \pm 0.01$ and ± 0.1 (impedance changes of $\pm 1\%$ and $\pm 10\%$) are shown in Fig. 7.

Appendix C
Partial Derivatives of ϵ_r

The partial derivatives of the extracted ϵ_r with respect to the variables $W, t_T, t_m, Z_0, \rho, \rho_{sc}$, and ρ_{off} are given here. The calculation of these derivatives is done using (2), (8), and the chain rule for differentiation, i.e., for example

$$\frac{\partial\epsilon_r}{\partial x} = \frac{\partial\epsilon_r}{\partial\sqrt{\epsilon_r}}\frac{\partial\sqrt{\epsilon_r}}{\partial x} \tag{19}$$

where x represents any of $W, t_T, t_m, Z_0, \rho, \rho_{sc}$, and ρ_{off}. Also, since $\partial\epsilon_r/\partial Z_0, \partial\epsilon_r/\partial\rho, \partial\epsilon_r/\partial\rho_{sc}$, and $\partial\epsilon_r/\partial\rho_{\text{off}}$ have a common factor, namely $\partial\epsilon_r/\partial Z_T$, we will use this factor and the partials of Z_T with respect to the appropriate variable. The following are the required partial derivatives:

$$\frac{\partial\epsilon}{\partial\sqrt{\epsilon_r}} = 2\sqrt{\epsilon_r} \tag{20}$$

$$\frac{\partial\sqrt{\epsilon_r}}{\partial W} = \pi(t_T-2t_m)\cosh^{-1}\left(\frac{t_T-t_m}{t_m}\right)\cdot\frac{Z_T-120\cosh^{-1}\left(\frac{t_T-t_m}{t_m}\right)}{Z_T\left[\pi(t_T-2t_m)+W\cosh^{-1}\left(\frac{t_T-t_m}{t_m}\right)\right]^2} \tag{21}$$

$$\frac{\partial\sqrt{\epsilon_r}}{\partial t_T} = \frac{\pi}{Z_T\left[\pi(t_T-2t_m)+W\cosh^{-1}\left(\frac{t_T-t_m}{t_m}\right)\right]}\cdot\left[120\cosh^{-1}\left(\frac{t_T-t_m}{t_m}\right)-Z_T + \frac{120\sqrt{t_T-2t_m}}{\sqrt{t_T}} - \frac{(t_T-2t_m)\left[120\cosh^{-1}\left(\frac{t_T-t_m}{t_m}\right)-Z_T\right]}{\pi(t_T-2t_m)+W\cosh^{-1}\left(\frac{t_T-t_m}{t_m}\right)}\cdot\frac{\pi\sqrt{t_T^2-2t_Tt_m}+W}{\sqrt{t_T^2-2t_Tt_m}}\right] \tag{22}$$

$$\frac{\partial\sqrt{\epsilon_r}}{\partial t_m} = \frac{2\pi}{Z_T\left[\pi(t_T-2t_m)+W\cosh^{-1}\left(\frac{t_T-t_m}{t_m}\right)\right]}\cdot\left[Z_T-120\cosh^{-1}\left(\frac{t_T-t_m}{t_m}\right) - \frac{120\sqrt{t_T^2-2t_Tt_m}}{t_m}\right.$$

$$- \frac{(t_T - 2t_m)\left[120\cosh^{-1}\left(\frac{t_T - t_m}{t_m}\right) - Z_T\right]}{\pi(t_T - 2t_m) + W\cosh^{-1}\left(\frac{t_T - t_m}{t_m}\right)} \cdot \frac{2\pi t_m\sqrt{t_T^2 - 2t_T t_m} - t_T W}{t_m\sqrt{t_T^2 - 2t_T t_m}}\Bigg] \tag{23}$$

$$\frac{\partial\sqrt{\epsilon_r}}{\partial Z_T} = -120\pi(t_T - 2t_m) \cdot \frac{\cosh^{-1}\left(\frac{t_T - t_m}{t_m}\right)}{Z_T^2\left[\pi(t_T - 2t_m) + W\cosh^{-1}\left(\frac{t_T - t_m}{t_m}\right)\right]} \tag{24}$$

$$\frac{\partial Z_T}{\partial Z_0} = \frac{1 - \rho'}{1 + \rho'} \tag{25}$$

$$\frac{\partial Z_T}{\partial \rho'} = \frac{2Z_0}{(1 - \rho')^2} \tag{26}$$

$$\frac{\partial \rho'}{\partial \rho} = \frac{1}{(\rho_{\text{off}} - \rho_{sc})^2} \tag{27}$$

$$\frac{\partial \rho'}{\partial \rho_{sc}} = \frac{\rho - \rho_{\text{off}}}{(\rho_{\text{off}} - \rho_{sc})^2} \tag{28}$$

and

$$\frac{\partial \rho}{\partial \rho_{\text{off}}} = \frac{\rho_{sc} - \rho}{(\rho_{\text{off}} - \rho_{sc})^2}. \tag{29}$$

ACKNOWLEDGMENT

The author would like to thank T. Leedy of the Advanced Technology Program of NIST for supporting this work and R. M. Japp of IBM Microelectronics, Endicott, NY, for providing PWB samples. The author is also grateful to R. H. Palm of NIST-Gaithersburg for preparing and measuring the samples and to B. A. Bell of NIST-Gaithersburg for editorial and administrative support.

REFERENCES

[1] L. P. Lightart, "A fast computational technique for accurate permittivity determination using transmission line methods," *IEEE Trans. Microwave Theory Tech.*, vol. MTT-31, p. 249, 1983.

[2] W. B. Weir, "Automatic measurement of complex dielectric constant and permeability at microwave frequencies," *Proc. IEEE*, vol. 62, p. 33, 1974.

[3] G. Kent, "A dielectrometer for the measurement of substrate permittivity," *Microwave J.*, p. 72, 1991.

[4] A. B. Bereskin, "Microwave dielectric property measurements," *Microwave J.*, p. 98, July 1992.

[5] G. Chen, K. Li, and Z. Ji, "Bilayered dielectric measurement with an open-ended coaxial probe," *IEEE Trans. Microwave Theory Tech.*, vol. 42, p. 966, 1994.

[6] S. S. Stuchly, C. L. Sibbald, and J. M. Anderson, "A new aperture admittance model for open-ended waveguides," *IEEE Trans. Microwave Theory Tech.*, vol. 42, p. 192, 1994.

[7] B. Tian and W.R. Tinga, "A microwave oscillation loop for dielectric constant measurement," *Trans. Microwave Theory Tech.*, vol. 42, p. 169, 1994.

[8] J. Baker-Jarivs, E. J. Vanzura, and W. A. Kissick, "Improved technique for determining complex permittivity with the transmission/reflection method," *IEEE Trans. Microwave Theory Tech.*, vol. 38, p. 1096, 1990.

[9] J. Baker-Jarvis, M. D. Janezic, J. H. Grosvenor, and R. G. Geyer, *Transmission/Reflection and Short-circuit Line Methods for Measuring Permittivity and Permeability,* NIST Technical Note 1355-R, U.S. Government Printing Office, Washington, D.C., 1993.

[10] H. Fellner-Feldegg, "The measurement of dielectrics in the time domain," *J. Phys. Chem.*, vol. 73, p. 616, 1969.

[11] A. M. Nicolson and G. F. Ross, "Measurement of the intrinsic properties of materials by time-domain techniques," *IEEE Trans. Instrum. Meas.*, vol. IM-19, p. 377, 1970.

[12] B. P. Kwok, S. O. Nelson, and E. Bahar, "Time-domain measurements for determination of dielectric properties of agricultural materials," *IEEE Trans. Instrum. Meas.*, vol. IM-28, p. 109, 1979.

[13] C. Boned and J. Peyrelasse, "Automatic measurement of complex permittivity (from 2 MHz to 8 GHz) using time domain spectroscopy," *J. Phys. E: Sci. Instrum.*, vol. 15, p. 534, 1982.

[14] R. Chahine and T. K. Bose, "Measurement of small dielectric loss by time-domain spectroscopy: Applications to water/oil emulsions," *IEEE Trans. Instrum. Meas.*, vol. IM-32, p. 360, 1983.

[15] S. A. Areone and R. Wills, "A numerical study of dielectric measurements using single-reflection time-domain reflectometry," *J. Phys. E: Sci. Instrum.*, vol 19, p. 447, 1986.

[16] R. H. Cole, "Evaluation of dielectric behavior by time domain spectroscopy. 1. Dielectric response by real time analysis," *J. Phys. Chem.*, vol. 79, p. 1459, 1975.

[17] M. El Kadiri, J. P. Parneix, and A. Chapoton, "General time domain analysis of T.D.S. data: Application to liquid crystals," *IEEE Trans. Instrum. Meas.*, vol. IM-34, p. 70, 1985.

[18] S. Ramo, J. R. Whinnery, and T. Van Duzer, *Fields and Waves in Communication Electronics,* 2nd ed. New York: Wiley, 1984.

[19] H. H. Ku, "Notes on the use of propagation of error formulas," *J. Res. NBS*, vol 70-C, p. 263, 1966.

Nicholas G. Paulter received the M.S. degree in chemistry from the University of New Mexico, Albuquerque, in 1988, and the M.S. degree in electrical engineering from the University of Colorado, Boulder, in 1990.

He was with the Los Alamos National Laboratory, Los Alamos, NM, from 1980 to 1989, and was involved in the study of fast electrical phenomena and in the development of high-speed photoconductors for use as ultrafast light detectors and sampling gates. In 1989, he joined the National Institute of Standards and Technology (NIST), Boulder, CO, to develop transient pulse measurement techniques and analysis. He is presently with NIST, Gaithersburg, MD. His present research interests include semiconductor physics, material properties, electro-optics, ultrafast electronic phenomena, and waveform/data processing and analysis.